Photoemission study of the electronic structure of the Kondo lattices $Yb_2Pt_6X_{15}$ (X=Al, Ga)

Awabaikeli Rousuli,[1,*] Shogo Nakamura,[2] Hitoshi Sato,[3,†] Takuya Ueda,[4] Yuji Matsumoto,[4,‡] Shigeo Ohara,[4] Eike F. Schwier,[3] Toshiki Nagasaki,[1] Kojiro Mimura,[5] Hiroaki Anzai,[5] Katsuya Ichiki,[5] Shigenori Ueda,[6,7] Kenya Shimada,[3] Hirofumi Namatame,[3] and Masaki Taniguchi[3]

[1]*Graduate School of Science, Hiroshima University, Higashi-Hiroshima 739-8526, Japan*
[2]*Department of Materials Science and Engineering, Tokyo Institute of Technology, Yokohama 226-8502, Japan*
[3]*Hiroshima Synchrotron Radiation Center, Hiroshima University, Higashi-Hiroshima 739-0046, Japan*
[4]*Graduate School of Engineering, Nagoya Institute of Technology, Nagoya 466-8555, Japan*
[5]*Graduate School of Engineering, Osaka Prefecture University, Sakai 599-8531, Japan*
[6]*Synchrotron X-ray Station at SPring-8, National Institute for Materials Science, Hyogo 679-5148, Japan*
[7]*Quantum Beam Unit, National Institute for Materials Science, Tsukuba 305-0047, Japan*

(Received 22 February 2017; revised manuscript received 8 June 2017; published 14 July 2017)

The electronic structure of Yb-based Kondo lattices $Yb_2Pt_6X_{15}$ (X=Al, Ga) has been investigated by means of photoemission spectroscopy using hard x-ray ($h\nu = 5.95$ keV) and vacuum ultraviolet ($h\nu = 182$ eV) synchrotron radiation. The Yb $3d$ spectra of $Yb_2Pt_6X_{15}$ showed both Yb^{2+}- and Yb^{3+}-derived structures, directly indicating valence fluctuation. The Yb valences of $Yb_2Pt_6Al_{15}$ were estimated to be 2.89 ± 0.01 at 250 K and ~2.83 at 20 K, while those of $Yb_2Pt_6Ga_{15}$ were ~2.34 at 300 K with almost no temperature dependence. With changing X ions from Al to Ga, the Pt $5d$ and Pt $4f$ peaks were shifted to shallower binding energies, and the Yb^{3+} $4f$ peaks were shifted to the deeper binding energies. The X dependences of the Yb valence and the Kondo temperature of $Yb_2Pt_6X_{15}$ are discussed based on the Yb^{3+} $4f$ hole level relative to the Fermi level E_F and Pt-derived density of states at E_F.

DOI: 10.1103/PhysRevB.96.045117

I. INTRODUCTION

Yb-based Kondo lattices show a wide variety of intriguing physical properties such as heavy-fermion behavior, valence fluctuation, and superconductivity. The ground state in such systems is believed to be qualitatively determined by the competition between the intersite Ruderman-Kittel-Kasuya-Yosida (RKKY) interaction and the on-site Kondo effect, both arising from the hybridization between the localized Yb $4f$ electrons and itinerant conduction electrons (c-f hybridization). When the RKKY interaction is dominant, the $4f$ electrons interact indirectly with each other mediated by the conduction electrons, and a magnetic ordered state is realized at low temperature. On the other side, when the Kondo effect is dominant, the $4f$ moments are screened by the conduction electrons, leading to a nonmagnetic Fermi-liquid ground state. This situation is summarized in the so-called Doniach phase diagram [1]. The boundary point at zero temperature separating the magnetic and nonmagnetic ground-state regions defines the quantum critical point (QCP).

The Kondo lattices $Yb_2Pt_6X_{15}$ (X=Al, Ga) have a quasi-two-dimensional $Sc_{1.2}Fe_4Si_{9.8}$-type crystal structure with space group $P6_3/mmc$ [2] or $Cmcm$ [3]. Several transport measurements were carried out for $Yb_2Pt_6Al_{15}$ [2]. The magnetic susceptibility at high temperature shows the Curie-Weiss behavior with an effective magnetic moment of $\mu_{\rm eff} \sim 4.1\mu_B$, close to the value of the free Yb^{3+} ion. After reaching its maximum at $T_{\rm max} \sim 30$ K, the susceptibility drops and becomes almost temperature independent at lower temperature with a paramagnetic ground state. The experimental data are well fitted with the Coqblin-Schrieffer model for $J = 7/2$ of Yb^{3+} with a Kondo temperature of $T_K = 64$ K [2].

The physical properties of $Yb_2Pt_6Ga_{15}$ have not been reported except for the lattice constant and heat-capacity measurements on a series of $R_2Pt_6Ga_{15}$ (R = rare earth) [4]. The lattice constants of $Yb_2Pt_6Ga_{15}$ deviate to larger values from the monotonic shrink curve from R = La to Lu expected from the lanthanide contraction, suggesting a nearly divalent Yb in this compound. From the magnetic susceptibility measurements (see Fig. 3 below), T_K is suggested to be higher than 1000 K.

Utsumi *et al.* investigated the electronic structure of the Kondo lattices $YbNi_3X_9$ by means of hard x-ray photoemission spectroscopy (HAXPES) [5]. Its crystal structure is $ErNi_3X_9$ type (space group $R32$), similar to that of $Yb_2Pt_6X_{15}$, as described later. In spite of the same crystal structure and similar nominal electron configurations (Al $3s^23p^1$ and Ga $4s^24p^1$), $YbNi_3Al_9$ exhibits a chiral helical order with a Néel temperature of $T_N = 3.4$ K [6], while $YbNi_3Ga_9$ exhibits valence fluctuation within the nonmagnetic ground state [7,8]. The T_K values of $YbNi_3X_9$ change from 2.7 K for $YbNi_3Al_9$ to 570 K for $YbNi_3Ga_9$. Thus, depending on X, $YbNi_3X_9$ is located in different phases separated by the QCP in the Doniach phase diagram. It should be noted, however, that $YbNi_3Ga_9$ shows pressure-induced antiferromagnetic order at 9 GPa [9], demonstrating its state being close to the QCP. Based on the HAXPES results, Utsumi *et al.* interpreted that the increased Ni $3d$ density of states (DOS) at E_F and the $4f$ hole level closer to E_F for $YbNi_3Ga_9$ lead to an increase in T_K and induce the strong valence fluctuation [5].

Although $Yb_2Pt_6X_{15}$ compounds are located in the nonmagnetic region of the phase diagram, the X dependence

*d144409@hiroshima-u.ac.jp
†jinjin@hiroshima-u.ac.jp
‡Present address: Graduate School of Science and Engineering, University of Toyama, Toyama 930-8555, Japan.

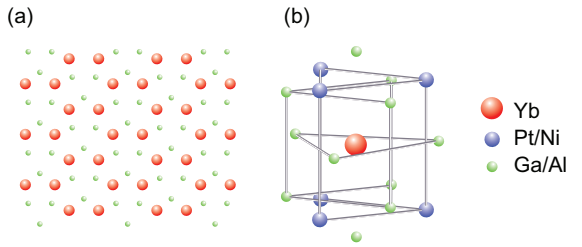

FIG. 1. (a) Yb_2X_3 layer and (b) local coordination around the Yb ion of $Yb_2Pt_6X_{15}$ and $YbNi_3X_9$.

of T_K similar to that for $YbNi_3X_9$ indicates that $Yb_2Pt_6X_{15}$ compounds occupy different positions: close to the QCP for $Yb_2Pt_6Al_{15}$ but farther away from the QCP for $Yb_2Pt_6Ga_{15}$. In addition to the similar X dependences of T_K, the two systems have similar crystal structures in that the Yb_2X_3 layer shown in Fig. 1(a) is sandwiched between two X-Pt(Ni)-X layers as X-Pt(Ni)-X-Yb_2X_3-X-Pt(Ni)-X, where the X and Pt(Ni) layers form triangular lattices. This unit of layers stacks along the c axis in $Yb_2Pt_6X_{15}$, and the X layer is located between the two units of layers in $YbNi_3X_9$. The local coordination around the Yb ion is similar between the two systems, as shown in Fig. 1(b).

Pt and Ni have $5d$ and $3d$ electrons, respectively, and belong to the same family in the periodic table. The physical properties of $Yb_2Pt_6X_{15}$ and $YbNi_3X_9$ are expected to be interpreted mainly from the characters of the $5d$ and $3d$ bands. $Yb_2Pt_6X_{15}$ is thus a suitable system to extend the studies on $YbNi_3X_9$ and provides an opportunity to systematically investigate the relation between the electronic structure and physical properties of Yb compounds. In this study, we carry out HAXPES with $h\nu = 5.95$ keV and vacuum ultraviolet photoemission spectroscopy (VUVPES) with $h\nu = 182$ eV on $Yb_2Pt_6X_{15}$ and investigate the X dependence of the electronic structure in comparison with $YbNi_3X_9$ [5]. The HAXPES and VUVPES results reveal the similarity in the X dependences of the electronic structure between $Yb_2Pt_6X_{15}$ and $YbNi_3X_9$. The Yb $3d$ spectra show valence fluctuation behavior of $Yb_2Pt_6X_{15}$. The Yb valence of $Yb_2Pt_6Al_{15}$ decreases from 2.89 ± 0.01 ($T = 250$ K) to 2.83 ($T = 20$ K), while that of $Yb_2Pt_6Ga_{15}$ is ~2.34, with no significant temperature dependence. The Pt $5d$ and Pt $4f$ peaks of $Yb_2Pt_6Ga_{15}$ are shifted to the shallower binding energy E_B, while the Yb^{3+} $4f$ peaks are found at deeper E_B compared to those of $Yb_2Pt_6Al_{15}$. We explain the differences in the Yb valence and T_K in $Yb_2Pt_6X_{15}$ via the Yb^{3+} $4f$ hole level above the Fermi level E_F and the Pt-derived DOS at E_F by making comparisons to previous results of $YbNi_3X_9$ [5]. From the combined HAXPES results of $Yb_2Pt_6X_{15}$ and $YbNi_3X_9$ [5], we find correlations among T_K, the Yb valence, and Yb^{3+} $4f$ peak energy. We discuss the higher T_K for $Yb_2Pt_6X_{15}$ compared to $YbNi_3X_9$ based on the DOS at E_F derived from the broad Pt $5d$ band.

II. EXPERIMENTS

Single crystals of $Yb_2Pt_6X_{15}$ (X = Al, Ga) were synthesized by means of the self-flux method. The starting materials were mixed with a ratio of Yb:Pt:X = 1:3:30 and put in an alumina crucible sealed in an evacuated quartz tube. For

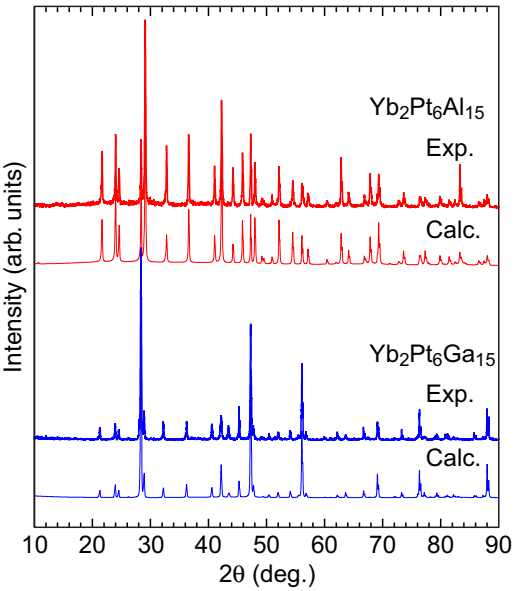

FIG. 2. XRD patterns (thick lines) of $Yb_2Pt_6X_{15}$ in comparison to calculated ones derived from the fits with the $Sc_{1.2}Fe_4Si_{9.8}$-type crystal structure (thin lines).

$Yb_2Pt_6Al_{15}$, the ampoule was heated to 1150 °C and kept at that temperature for 5 h. Then it was cooled to 850 °C over 1 h, again heated to 900 °C over 1 h, and cooled to 750 °C over 30 h. The excess Al was removed in a centrifuge and further washed out in a NaOH solution. The growth method of $Yb_2Pt_6Ga_{15}$ is described in Ref. [4]. The single phase of the grown sample was verified by x-ray powder diffraction (XRD). No XRD peak due to impurity phases was detected, as shown in Fig. 2.

Figure 3 shows the magnetic susceptibilities of $Yb_2Pt_6Ga_{15}$ under magnetic fields of 10 kOe measured using a superconducting quantum interference device magnetometer (Quantum Design). The two results under magnetic fields applied parallel to the a and c axes exhibit similar temperature dependences with weak anisotropy. The susceptibility continuously de-

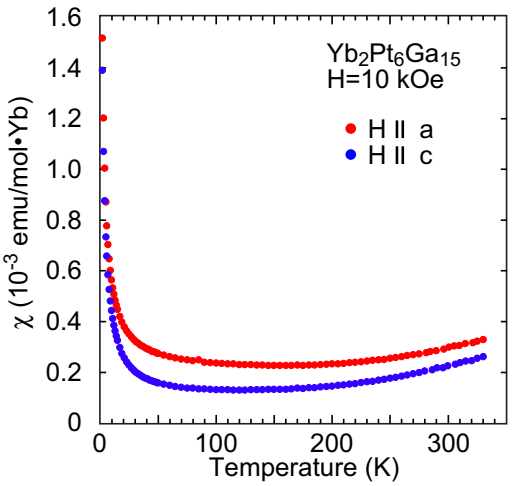

FIG. 3. Magnetic susceptibilities of $Yb_2Pt_6Ga_{15}$ under magnetic fields of 10 kOe parallel to the a and c axes.

creases on cooling from 330 K and becomes almost constant below 200 K. The ground state is paramagnetic, as is the case in $Yb_2Pt_6Al_{15}$. Based on these measurements and by scaling the susceptibility for $Yb_2Pt_6Al_{15}$, T_{max} in $Yb_2Pt_6Ga_{15}$ has to be located above 350 K, which in turn gives a lower limit for T_K of at least 1000 K from $3T_{max}$. Below 30 K, the magnetic susceptibilities rapidly increase, probably caused by a small amount of magnetic impurity, such as Yb_2O_3. However, the impurities were not identified within the XRD patterns in Fig. 2.

The HAXPES experiments were performed at undulator beamline BL15XU [10] of SPring-8. The excitation energy was $h\nu = 5.95$ keV monochromatized using a Si 111 double crystal and Si 333 channel-cut monochromators [11]. A high-energy-resolution hemispherical photoelectron analyzer (VG Scienta R4000) was used to collect the angle-integrated HAXPES spectra. The total energy resolution was set to 240 meV. The angle-integrated VUVPES spectra were measured with $h\nu = 182$ eV at bending beamline BL-7 of the Hiroshima Synchrotron Radiation Center (HSRC) equipped with a Dragon-type monochromator [12]. A hemispherical photoelectron analyzer (VG Scienta SES2002) was used, and the total energy resolution was set to 150 meV. E_B of the HAXPES and VUVPES spectra was calibrated by measuring the Fermi edge of polycrystalline Au. Clean surfaces were obtained by fracturing *in situ*.

III. RESULTS AND DISCUSSION

It is well known that line shape analysis of the Yb 3*d* HAXPES spectra provides the mean Yb valence with high accuracy [13]. Temperature-dependent Yb 3*d* spectra from $Yb_2Pt_6Al_{15}$ and $Yb_2Pt_6Ga_{15}$ are displayed in Figs. 4(a) and 4(b), respectively. The Yb 3*d* spectra are composed of the $3d_{5/2}$ part at 1515–1540 eV and $3d_{3/2}$ part at 1560–1590 eV [see Fig. 4(b)]. In the case of $Yb_2Pt_6Al_{15}$, an intense Al 1*s* peak is visible at 1559.5 eV, and the tail strongly disturbs the spectral feature in the $3d_{3/2}$ region. Therefore, we measured only the $3d_{5/2}$ spectra for $Yb_2Pt_6Al_{15}$, as shown in Fig. 4(a).

The Yb $3d_{5/2}$ spectra of $Yb_2Pt_6Al_{15}$ exhibit clear temperature dependence between 250 and 20 K. The spectral feature is similar to that of other Yb compounds [5,13–15]. With decreasing temperature, the Yb^{2+}-derived single peak at 1520 eV is gradually enhanced, while the Yb^{3+}-derived multiplet structures due to the $3d^9 4f^{13}$ final states at 1524–1536 eV are reduced. The temperature dependence of the spectra indicates that the Yb valence is shifted to the divalent side at low temperature, which is clear evidence of valence fluctuation in $Yb_2Pt_6Al_{15}$.

In contrast, the temperature dependence of the Yb 3*d* spectra of $Yb_2Pt_6Ga_{15}$ in Fig. 4(b) is much weaker. The $3d_{3/2}$ region is also divided into the Yb^{2+} peak at 1568 eV and Yb^{3+} multiplet structures at 1574–1582 eV. The intensities of the Yb^{3+} structures are significantly weak compared to the Yb^{2+} peaks, indicating the Yb ion in $Yb_2Pt_6Ga_{15}$ is closer to divalent. The weak structures shown by the vertical bars at 1537 and 1584 eV come from the Yb^{2+}-derived plasmon satellites [5].

Since the Yb^{2+} and Yb^{3+} components are clearly resolved in the Yb 3*d* spectrum, the Yb valence can be precisely deduced from their integral intensity ratio. In order to estimate

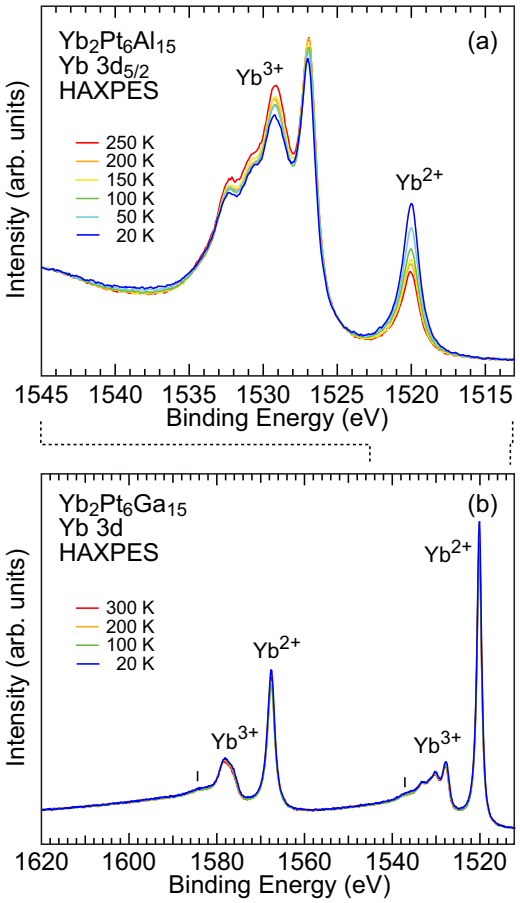

FIG. 4. (a) Temperature dependences of Yb $3d_{5/2}$ HAXPES spectra of $Yb_2Pt_6Al_{15}$ measured between 250 and 20 K. (b) Temperature dependences of Yb 3*d* HAXPES spectra of $Yb_2Pt_6Ga_{15}$ measured between 300 and 20 K. Vertical bars indicate the plasmon satellite structures.

the Yb valence, we fitted the Yb 3*d* spectra with the procedure described in Ref. [13]. The fit of the spectrum of $Yb_2Pt_6Ga_{15}$ measured at 20 K is shown in Fig. 5(a) as an example. In the decomposed spectrum in the lower part, the broad curves around 1544 and 1597 eV correspond to the Yb^{3+}-derived plasmon satellites. The evaluated Yb valences of $Yb_2Pt_6X_{15}$ are summarized in Fig. 5(b). The Yb valence of $Yb_2Pt_6Al_{15}$ is 2.89 ± 0.01 at 250 K and gradually decreases on cooling to 2.83 at 20 K. On the other hand, the valence of $Yb_2Pt_6Ga_{15}$ is $\sim$2.34 in whole temperature range. The different temperature dependences of the valence in the two compounds can qualitatively be interpreted from their different T_K. According to a theoretical calculation using the noncrossing approximation, the Yb valence changes significantly around T_K [16]. Since T_K in $Yb_2Pt_6Al_{15}$ is $\sim$60K [2], its valence changes within the measured temperature region, while that of $Yb_2Pt_6Ga_{15}$ with $T_K > 1000$ K is almost constant below 300 K. The constant Yb valence ($\sim$2.2) below 300 K is also reported for $YbAl_2$ with $T_K = 2000$–2600 K [17].

In order to examine the electronic states near E_F including the Yb $4f$ states, we measured the valence-band HAXPES spectra of $Yb_2Pt_6X_{15}$, as shown in Fig. 6(a). A dashed line on the spectrum of $Yb_2Pt_6Al_{15}$ represents that of $Yb_2Pt_6Ga_{15}$

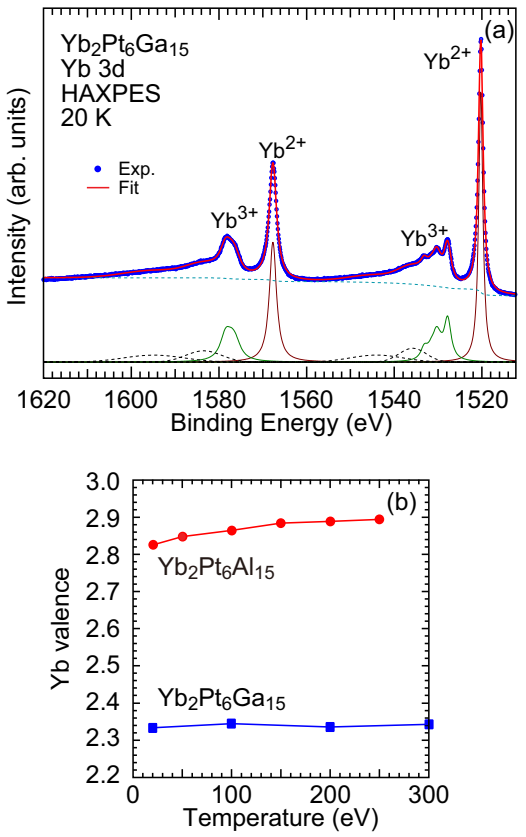

FIG. 5. (a) Fit of the Yb 3*d* HAXPES spectrum of $Yb_2Pt_6Ga_{15}$ measured at 20 K. (b) Yb valences of $Yb_2Pt_6X_{15}$ estimated from the fits of the spectra as a function of temperature.

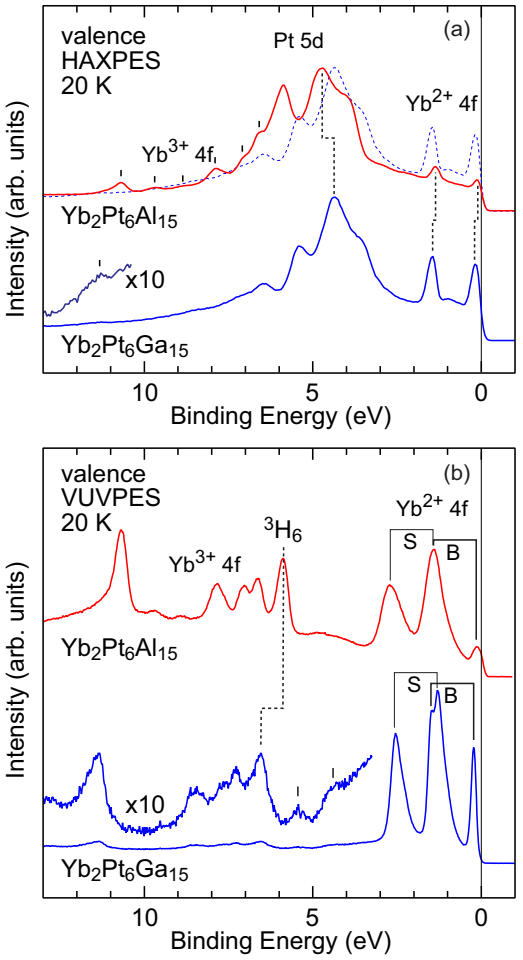

FIG. 6. (a) Valence-band HAXPES spectra of $Yb_2Pt_6X_{15}$ measured at 20 K. The dashed line on the spectrum of $Yb_2Pt_6Al_{15}$ represents that of $Yb_2Pt_6Ga_{15}$ for comparison. Vertical bars indicate the Yb^{3+} $4f$-derived peaks. (b) Valence-band VUVPES spectra of $Yb_2Pt_6X_{15}$ measured at 20 K. The bulk and surface Yb^{2+} $4f$ components are indicated with "B" and "S", respectively. Two peaks of the enlarged spectrum of $Yb_2Pt_6Ga_{15}$ shown by vertical bars correspond to those of the HAXPES spectrum.

normalized with the intense peak at 4–5 eV for comparison. Taking into account the photoionization cross sections at $h\nu =$ 6 keV [18], the spectra are mainly derived from the Pt 5*d*, Yb 4*f*, Ga 4*s*, and Al 3*s* states with a ratio of 14.5:2.6:3.3:1. Note that the delocalized *s* states are distributed in a wide E_B range, while the localized *d* and *f* states are in a narrow E_B range. The most prominent features at 3–6 eV are ascribed to the Pt 5*d* states, which is confirmed by the VUVPES spectra measured at $h\nu = 182$ eV [see Fig. 6(b)]. The Yb^{2+} $4f_{7/2}$ and $4f_{5/2}$ states are observed in the vicinity of E_F with a spin-orbit splitting of about 1.3 eV. On the other hand, the Yb^{3+} $4f$ multiplet structures due to the $4f^{12}$ final states are buried in the intense Pt 5*d* peak above 5 eV. Some Yb^{3+} $4f$ peaks are observed in the $Yb_2Pt_6Al_{15}$ spectrum, as indicated by vertical bars. Almost no structure is found in the $Yb_2Pt_6Ga_{15}$ spectrum in the corresponding region, reflecting that the Yb valence is close to divalent. Only one peak is very weakly detected at 11.3 eV, as we see in the enlarged spectrum in Fig. 6(a). This peak is considered to correspond to the peak at 10.7 eV in the $Yb_2Pt_6Al_{15}$ spectrum.

In order to clearly detect the Yb^{3+} $4f$ multiplet structures, in particular, for $Yb_2Pt_6Ga_{15}$, we measured valence-band VUVPES spectra at $h\nu = 182$ eV, where the Yb^{3+} $4f$ structures are enhanced by the Yb $4d$-$4f$ resonance [19]. The VUVPES spectra of $Yb_2Pt_6X_{15}$ are compared in Fig. 6(b). Due to the resonant enhancement, we clearly see the Yb^{3+} $4f$ multiplet structures at 5–13 eV, in particular, in the $Yb_2Pt_6Al_{15}$ spectrum. The overall feature including the relative intensity is consistent with that observed for other Yb compounds [20]. The shallowest peak at 5.8 eV, which is completely overlapped by the Pt 5*d* peak in the HAXPES spectrum in Fig. 6(a), is ascribed to the $^3H_6$ multiplet. Although the Yb^{3+} $4f$ structures are still weak in the $Yb_2Pt_6Ga_{15}$ spectrum, they are clearly observed in the enlarged spectrum. A peak at 6.5 eV is attributed to the $^3H_6$ multiplet, and a peak at 11.3 eV corresponds to the 10.7 eV peak in the $Yb_2Pt_6Al_{15}$ spectrum.

The Yb^{2+} $4f$ region between E_F and 3.5 eV in the VUVPES spectra is composed of the surface components as well as the bulk components because of the surface sensitivity of VUVPES. The peak just below E_F is due to bulk Yb $4f_{7/2}$ states, as observed in the bulk-sensitive HAXPES spectra in Fig. 6(a). In contrast, the peak around 2.5–3.0 eV is due to surface $4f_{5/2}$ states since they are not detected in the HAXPES spectra. The bulk $4f_{5/2}$ and surface $4f_{7/2}$ states contribute to the structure around 1.3 eV and are resolved

in the case of $Yb_2Pt_6Ga_{15}$; the shallower peak at 1.3 eV is derived from the surface $4f_{7/2}$ states, and the shoulder at 1.45 eV is derived from the bulk $4f_{5/2}$ states. We see that the bulk- and surface-originated electronic states almost equally contribute to the VUVPES spectra from their intensity ratio. Both components should also contribute to the Yb^{3+} $4f$ spectra, although they are not resolved. The Yb^{3+} $4f$ peaks of $YbRh_2Si_2$ measured at $h\nu = 115$–800 eV are clearly split into the bulk and surface components, and the bulk-derived peak is located at 0.11 eV shallower E_B than the surface-derived peak [21].

There is almost no structure around 5 eV in the VUVPES spectra of both compounds. As indicated by vertical bars in the enlarged spectrum of $Yb_2Pt_6Ga_{15}$, the two peaks are detected at corresponding energies of the Pt $5d$-attributed peaks in the HAXPES spectrum. Already in the off-resonant case, the contribution by the Pt $5d$, Ga $4s$, and Al $3s$ states to the spectra is less than 5% compared to Yb $4f$ at $h\nu = 180$ eV [22]. The Yb $4f$ signal is further increased by the resonant condition, making Yb $4f$ the dominant contribution. The VUVPES therefore clarifies that the most noticeable peak at 3–6 eV in the HAXPES spectra originates from the Pt $5d$ states.

The Yb^{2+} $4f$ peaks of $Yb_2Pt_6Ga_{15}$ are located away from E_F compared to $Yb_2Pt_6Al_{15}$. Since the Yb^{2+} $4f_{7/2}$ peak is assigned to the Kondo peak [17], the deeper E_B reflects the higher T_K in $Yb_2Pt_6Ga_{15}$; the peak position of 0.18 eV corresponds to $T_K \sim 2100$ K. The Yb^{3+} $4f$ multiplet structures for $Yb_2Pt_6Ga_{15}$ are also shifted to deeper E_B by $\Delta E_B = 0.6$ eV. Its energy position is related to the Yb^{3+} $4f$ hole level ($\varepsilon_f > 0$) above E_F, as discussed in Ref. [5]. In the multielectron picture, ε_f corresponds to the energy for the $f^{13} \rightarrow f^{14}$ transition, and the Yb^{3+} $4f$ peaks in the photoemission spectra ($f^{13} \rightarrow f^{12}$ transition) are roughly located at $-\varepsilon_f + U$, with U being the Coulomb repulsion energy between the $4f$ holes in the f^{12} final states. Since U is expected to be almost intra-atomic and unchanged between $Yb_2Pt_6Al_{15}$ and $Yb_2Pt_6Ga_{15}$, the deeper E_B of the Yb^{3+} $4f$ peaks for $Yb_2Pt_6Ga_{15}$ suggests smaller ε_f, that is, the Yb^{3+} $4f$ hole level being closer to E_F. This observation is consistent with the nearly divalent Yb in $Yb_2Pt_6Ga_{15}$ because of the lower energy required for the transfer of the conduction electrons to the Yb^{3+} $4f$ hole. In the Pt $5d$ peak a shift to shallower E_B by $\Delta E_B = 0.3$ eV is detected for $Yb_2Pt_6Ga_{15}$.

In order to investigate the X dependence of the conduction states from the peak shift of the core levels, we measured the Pt $4f$ HAXPES spectra of $Yb_2Pt_6X_{15}$ at 20 K, as shown in Fig. 7. The Pt $4f_{7/2}$ and $4f_{5/2}$ peaks of $Yb_2Pt_6Ga_{15}$ are located at 72.0 and 75.4 eV, respectively, with shallower E_B than those of $Yb_2Pt_6Al_{15}$ by $\Delta E_B = 0.3$ eV. The direction of the energy shift is the same as observed for the Pt $5d$ peaks in Fig. 6(a), and their amounts are comparable, which indicates that the E_F position of the conduction-band DOS moves to the lower-energy side on going from $Yb_2Pt_6Al_{15}$ to $Yb_2Pt_6Ga_{15}$.

The HAXPES results of $Yb_2Pt_6X_{15}$ are comparable to those previously reported for $YbNi_3X_9$ [5] with a similar X dependence of T_K (2.7 K for $YbNi_3Al_9$ and 570 K for $YbNi_3Ga_9$ [7,8]). Note again that $Yb_2Pt_6X_{15}$ and $YbNi_3X_9$ possess similar crystal structures and local coordinates around the Yb ion. Yb $3d$ HAXPES revealed that $YbNi_3Ga_9$ exhibits

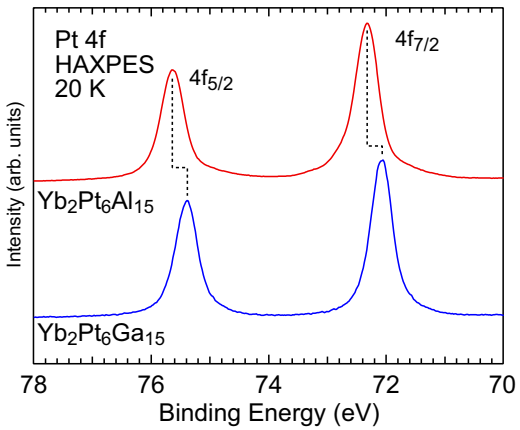

FIG. 7. Pt $4f$ HAXPES spectra of $Yb_2Pt_6X_{15}$ measured at 20 K.

strong valence fluctuation behavior with Yb valences of 2.59 at 300 K and 2.43 at 22 K. The valence of $YbNi_3Al_9$ is nearly 3 (~2.97), with little temperature dependence. In both systems, the valence is shifted to the divalent side with exchanging Al with Ga.

Similar X dependences are observed in the core level and valence-band HAXPES spectra as well as the Yb valence for $Yb_2Pt_6X_{15}$ and $YbNi_3X_9$. Figures 8(a) and 8(b) exhibit the Ni $2p_{3/2}$ and valence-band spectra of $YbNi_3X_9$, respectively [5], and Figs. 8(c) and 8(d) show the Pt $4f_{7/2}$ and valence-band spectra of $Yb_2Pt_6X_{15}$ for comparison. The Ni $2p_{3/2}$ peak of $YbNi_3Ga_9$ is shifted to shallower E_B by $\Delta E_B = 0.3$ eV, and

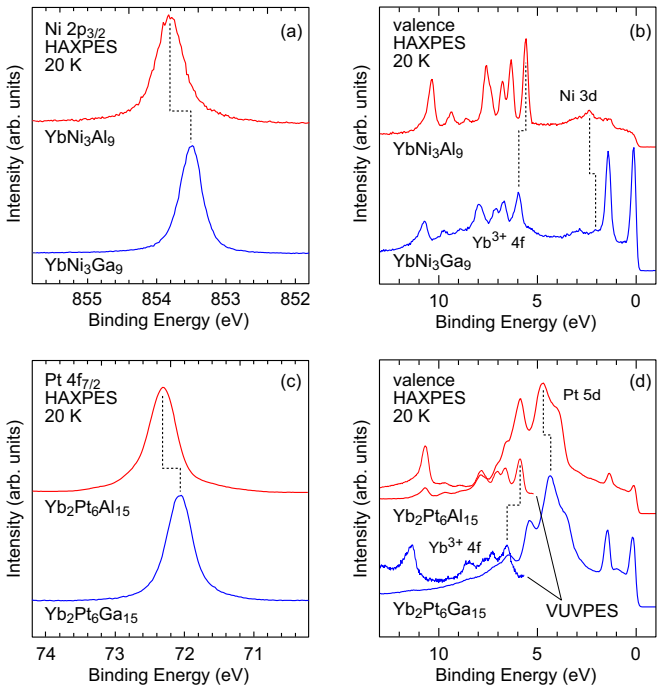

FIG. 8. Comparison of HAXPES spectra measured at 20 K between $Yb_2Pt_6X_{15}$ and $YbNi_3X_9$. (a) Ni $2p_{3/2}$ and (b) valence-band spectra of $YbNi_3X_9$, and (c) Pt $4f_{7/2}$ and (d) valence-band spectra of $Yb_2Pt_6X_{15}$. Thin lines in (d) depict VUVPES spectra in the Yb^{3+} $4f$ region.

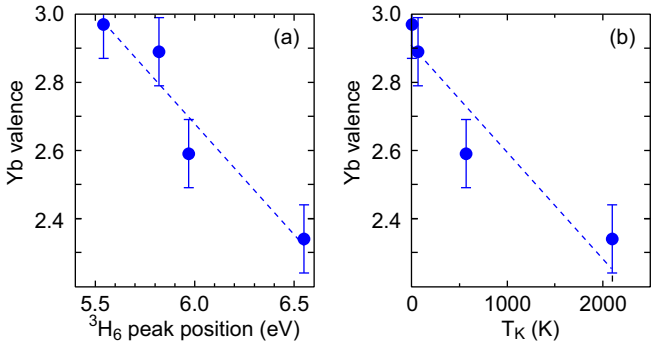

FIG. 9. Yb valence plotted for (a) the $^3H_6$ peak position and (b) T_K for $Yb_2Pt_6X_{15}$ together with those of $YbNi_3X_9$ [5]. Dashed lines are guides for eye.

so is the Ni $3d$ peak within the valence bands. By contrast, the Yb^{3+} $4f$ multiplet structures exhibit an opposite energy shift by $\Delta E_B = 0.4$ eV. Based on the HAXPES results, Utsumi *et al.* described the X dependence of physical properties of $YbNi_3X_9$ by the differences of the Ni $3d$ DOS at E_F and the Yb^{3+} $4f$ hole level relative to E_F [5]. The increased Ni $3d$ DOS at E_F and the $4f$ hole level closer to E_F for $YbNi_3Ga_9$ enhance the c-f hybridization, that is, increase T_K and induce the strong valence fluctuation.

The X dependences of the Yb valence and the energy shifts in the Pt $4f$, Pt $5d$, and Yb^{3+} $4f$ peaks found for $Yb_2Pt_6X_{15}$ are similar to those for $YbNi_3X_9$ [5]. For both cases, the substitution of an X ion from Al to Ga decreases the Yb valence and shifts the Pt $4f$ and Pt $5d$ (Ni $2p_{3/2}$ and Ni $3d$) peaks toward shallower E_B and the Yb^{3+} $4f$ peaks toward deeper E_B. In line with the argument for $YbNi_3X_9$ [5], the increased Pt $5d$ DOS at E_F and Yb^{3+} $4f$ hole level closer to E_F for $Yb_2Pt_6Ga_{15}$ increase the c-f hybridization and T_K and decrease the Yb valence. Although the Pt $5d$ states mainly distribute at 3–6 eV in Fig. 6(a), we see that the Pt $5d$ DOS has a long tail toward E_F. Assuming a similar tail feature for both compounds, $Yb_2Pt_6Ga_{15}$ with its shallower Pt $5d$ peak is expected to have a larger Pt $5d$ DOS at E_F, which might be reflected in the increased spectral intensity around 1 eV in $Yb_2Pt_6Ga_{15}$. The similarities between the X-dependent spectra of $YbNi_3X_9$ and $Yb_2Pt_6X_{15}$ suggest some systematic changes in the electronic structure when compounds with the same crystal structure and similar conduction electron states move from nonmagnetic to magnetic regions in the Doniach phase diagram. The same trend is also found for antiferromagnetic $YbNiSi_3$ and nonmagnetic $YbNiGe_3$ [23].

Finally, we compare the electronic structures of $Yb_2Pt_6X_{15}$ and $YbNi_3X_9$ [5]. Here, recall T_K in these materials is 2.7 K for $YbNi_3Al_9$, 64 K for $Yb_2Pt_6Al_{15}$, 570 K for $YbNi_3Ga_9$, and higher than 1000 K for $Yb_2Pt_6Ga_{15}$, ~2100K derived from the Yb^{2+} $4f_{7/2}$ peak position. The difference in T_K is reflected well by the systematic changes in the Yb valence and the energy position of the $^3H_6$ peak. The valence at 300 K decreases in the order of $YbNi_3Al_9$ (2.97), $Yb_2Pt_6Al_{15}$ (2.89), $YbNi_3Ga_9$ (2.59), and $Yb_2Pt_6Ga_{15}$ (2.34), and the $^3H_6$ peak energies are 5.5, 5.8, 6.0, and 6.6 eV, respectively [24]. Figure 9(a) clearly indicates a correlation between the Yb valence and $^3H_6$ peak energy for $Yb_2Pt_6X_{15}$ and $YbNi_3X_9$. This trend can qualitatively be understood assuming that the deeper $^3H_6$ peak reflects the Yb^{3+} $4f$ hole level closer to E_F, as mentioned above. The conduction electrons are more readily transferred into the Yb^{3+} $4f$ hole, and the Yb valence is shifted to the divalent side. The Yb valence is also plotted for T_K in Fig. 9(b), and we notice that the valence is systematically shifted to the divalent side with increasing T_K. In order to quantitatively explain the correlation among T_K, the Yb valence, and $^3H_6$ peak energy, theoretical analyses of the spectra based on the single-impurity Anderson model with parameters such as the Yb $4f$ level, $4f$-$4f$ Coulomb interaction energy, and c-f hybridization energy are required.

The higher T_K in $Yb_2Pt_6X_{15}$ indicates that the c-f hybridization is larger than that for $YbNi_3X_9$. The larger c-f hybridization is reflected in $Yb_2Pt_6Al_{15}$ with no magnetic order, while $YbNi_3Al_9$ exhibits chiral helical order. Based on our observations, the increased Pt $5d$ and Ni $3d$ DOSs at E_F are important for describing the higher T_K in the Ga compounds. The Pt $5d$ DOS at E_F in $Yb_2Pt_6X_{15}$ is expected to be larger than the Ni $3d$ DOS at E_F in $YbNi_3X_9$. However, the Pt $5d$ peak is located at $E_B = 3$–6 eV, and the Ni $3d$ peak is located at $E_B \sim 2$ eV. If we assume that both DOS features have a similar tail toward E_F, the Pt $5d$ DOS at E_F should be lower than the Ni $3d$ DOS, which contradicts our expectation. Here, note that the Pt $5d$ DOS has a broader bandwidth than the Ni $3d$ DOS. In general, the Pt $5d$ states are relatively delocalized, while the Ni $3d$ states are relatively localized. In a photoemission study on Ni-Pt alloys, it was reported that the Pt $5d$ bands spread over the top 8 eV region in the valence bands, while the Ni $3d$ bands spread over the top 4 eV region [25]. Although the crystal structure is completely different between the Ni-Pt alloy and $Yb_2Pt_6X_{15}$ and $YbNi_3X_9$, the results are a measure of the Pt $5d$ and Ni $3d$ bandwidths. Thus, the broad bandwidth of the Pt $5d$ states may qualitatively explain the larger c-f hybridization and higher T_K in $Yb_2Pt_6X_{15}$. In order to clarify this point, a band-structure calculation based on the precise structural analysis is necessary in a future study.

IV. SUMMARY

The electronic structure of the Kondo lattices $Yb_2Pt_6X_{15}$ has been investigated by means of HAXPES with $h\nu = 5.95$ keV and VUVPES with $h\nu = 182$ eV. Both Yb^{2+}- and Yb^{3+}-derived structures were clearly observed in the Yb $3d$ spectra. For $Yb_2Pt_6Al_{15}$, the intensity of the Yb^{2+} (Yb^{3+}) structures gradually increases (decreases) with decreasing temperature. The estimated Yb valence of 2.89 at 250 K gradually decreases to 2.83 at 20 K. On the other hand, the Yb valence of $Yb_2Pt_6Ga_{15}$ is 2.34, with almost no temperature dependence. The Pt $4f$ and Pt $5d$ peaks are shifted to shallower E_B with changing the X ion from Al to Ga. At the same time, an energy shift toward deeper E_B in the Yb^{3+} $4f$ multiplet structures is observed. We described the enhanced c-f hybridization and T_K in $Yb_2Pt_6Ga_{15}$ based on the Pt-derived DOS at E_F and the Yb^{3+} $4f$ hole level relative to E_F together with results from $YbNi_3X_9$ [5]. Systematic changes with the same order of T_K were observed in the Yb valence and $^3H_6$ peak energy. We believe that the higher T_K for $Yb_2Pt_6X_{15}$ compared to $YbNi_3X_9$ is derived from the large Pt $5d$ DOS at E_F due to the broad bandwidth.

ACKNOWLEDGMENTS

The HAXPES experiments at SPring-8 were under the approval of the NIMS Synchrotron X-ray Station (Proposals No. 2014B4800, No. 2014B4902, No. 2015A4800, No. 2015A4906, No. 2015B4801, and No. 2015B4908). The VUVPES experiments at HSRC were performed under the approval of HSRC (Proposal No. 15-A-41). This work was partly supported by JSPS KAKENHI Grants No. 15K05174, No. 26400333, and No. 16H01073 (J-Physics) and by the NIMS microstructural characterization platform as a program of the "Nanotechnology Platform" (Project No. 12024046) of MEXT, Japan.

[1] S. Doniach, Physica B (Amsterdam) **91**, 231 (1977).
[2] M. Deppe, S. Hartmann, M. E. Macovei, N. Oeschler, M. Nicklas, and C. Geibel, New J. Phys. **10**, 093017 (2008).
[3] Y. Prots, M. Deppe, R. Cardoso-Gil, A. Cervellino, A. Ormeci, C. Geibel, and Y. Grin, Chem. Met. Alloys **7**, 85 (2014).
[4] Y. Matsumoto, T. Ueda, and S. Ohara, J. Phys. Conf. Ser. **683**, 012035 (2016).
[5] Y. Utsumi, H. Sato, S. Ohara, T. Yamashita, K. Mimura, S. Motonami, K. Shimada, S. Ueda, K. Kobayashi, H. Yamaoka, N. Tsujii, N. Hiraoka, H. Namatame, and M. Taniguchi, Phys. Rev. B **86**, 115114 (2012).
[6] S. Ohara, S. Fukuta, K. Ohta, H. Kono, T. Yamashita, Y. Matsumoto, and J. Yamaura, JPS Conf. Proc. **3**, 017016 (2014).
[7] T. Yamashita, R. Miyazaki, Y. Aoki, and S. Ohara, J. Phys. Soc. Jpn. **81**, 034705 (2012).
[8] S. Ohara, T. Yamashita, Y. Mori, and I. Sakamoto, J. Phys. Conf. Ser. **273**, 012048 (2011).
[9] K. Matsubayashi, T. Hirayama, T. Yamashita, S. Ohara, N. Kawamura, M. Mizumaki, N. Ishimatsu, S. Watanabe, K. Kitagawa, and Y. Uwatoko, Phys. Rev. Lett. **114**, 086401 (2015).
[10] S. Ueda, Y. Katsuya, M. Tanaka, H. Yoshikawa, Y. Yamashita, S. Ishimaru, Y. Matsushita, and K. Kobayashi, in *SRI 2009, 10th International Conference on Radiation Instrumentation*, AIP Conf. Proc. No. 1234 (AIP, New York, 2010), p. 403.
[11] K. Kobayashi, M. Yabashi, K. Tamasaku, D. Miwa, T. Ishikawa H. Nohira, T. Hattori, Y. Sugita, O. Nakatsuka, A. Sakai, and S. Zaima, Appl. Phys. Lett. **83**, 1005 (2003).
[12] M. Taniguchi and J. Ghijsen, J. Synchrotron Radiat. **5**, 1176 (1998).
[13] H. Sato, K. Shimada, M. Arita, K. Hiraoka, K. Kojima, Y. Takeda, K. Yoshikawa, M. Sawada, M. Nakatake, H. Namatame, M. Taniguchi, Y. Takata, E. Ikenaga, S. Shin, K. Kobayashi, K. Tamasaku, Y. Nishino, D. Miwa, M. Yabashi, and T. Ishikawa, Phys. Rev. Lett. **93**, 246404 (2004).
[14] L. Moreschini, C. Dallera, J. J. Joyce, J. L. Sarrao, E. D. Bauer, V. Fritsch, S. Bobev, E. Carpene, S. Huotari, G. Vankó, G. Manaco, P. Lacovig, G. Panaccione, A. Fondacaro, G. Paolicelli, P. Torelli, and M. Grioni, Phys. Rev. B **75**, 035113 (2007).
[15] H. Sato, Y. Utsumi, J. Kodama, M. Arita, H. Anzai, K. Mimura, K. Shimada, S. Ueda, N. Tsujii, H. Namatame, and M. Taniguchi, J. Phys. Conf. Ser. **592**, 012016 (2015).
[16] L. H. Tjeng, S.-J. Oh, E.-J. Cho, H.-J. Lin, C. T. Chen, G.-H. Gweon, J.-H. Park, J. W. Allen, T. Suzuki, M. S. Makivić, and D. L. Cox, Phys. Rev. Lett. **71**, 1419 (1993).
[17] M. Matsunami, A. Chainani, M. Taguchi, R. Eguchi, Y. Takata, M. Oura, M. Yabashi, K. Tamasaku, Y. Nishino, T. Ishikawa, M. Kosaka, and S. Shin, J. Phys. Soc. Jpn. **81**, 073702 (2012).
[18] J. H. Scofield, Lawrence Livemore Laboratory, Tech. Rep. No. UCRL-51326, 1973, doi:10.2172/4545040.
[19] H. Yamaoka, P. Thunström, N. Tsujii, I. Jarrige, K. Shimada, M. Arita, H. Iwasawa, H. Hayashi, J. Jiang, H. Namatame, M. Taniguchi, N. Hiraoka, H. Ishii, K.-D. Tsuei, M. Giovannini, and E. Bauer, Phys. Rev. B **86**, 085137 (2012).
[20] H. Sato, K. Yoshikawa, K. Hiraoka, M. Arita, K. Fujimoto, K. Kojima, T. Muro, Y. Saitoh, A. Sekiyama, S. Suga, and M. Taniguchi, Phys. Rev. B **69**, 165101 (2004).
[21] K. Kummer, Yu. Kucherenko, S. Danzenbächer, C. Krellner, C. Geibel, M. G. Holder, L. V. Bekenov, T. Muro, Y. Kato, T. Kinoshita, S. Huotari, L. Simonelli, S. L. Molodtsov, C. Laubschat, and D. V. Vyalikh, Phys. Rev. B **84**, 245114 (2011).
[22] J. J. Yeh and I. Lindau, At. Data Nucl. Data Tables **32**, 1 (1985).
[23] H. Sato, Y. Utsumi, J. Kodama, H. Nagata, M. A. Avila, R. A. Ribeiro, K. Umeo, T. Takabatake, K. Mimura, S. Motonami, H. Anzai, S. Ueda, K. Shimada, H. Namatame, and M. Taniguchi, Phys. Status Solidi C **12**, 620 (2015).
[24] These values for $Yb_2Pt_6X_{15}$ and $YbNi_3X_9$ are those of the VUVPES and HAXPES spectra, respectively. Both the bulk and surface electronic states contribute to the VUVPES spectra, and the bulk-originated $^3H_6$ peak energies of $Yb_2Pt_6X_{15}$ are possibly ∼0.1eV shallower according to Ref. [21], which does not affect the trend between the Yb valence and $^3H_6$ peak energies in Fig. 9(a).
[25] T. U. Nahm, J.-Y. Kim, S.-J. Oh, S.-M. Chung, J.-H. Park, J. W. Allen, K. Jeong, and S. Kim, Phys. Rev. B **54**, 7807 (1996).